

Shape control of simulated multi-segment continuum robots via Koopman operators with per-segment projection

Eron Ristich*, Jiahe Wang†, Lei Zhang†, Sultan Haidar Ali†, Wanxin Jin†, Yi Ren†, and Jiefeng Sun†‡

*Department of Electrical Engineering and Computer Science
University of Michigan, Ann Arbor, Michigan 48109, USA

†School for Engineering of Matter, Transport and Energy
Arizona State University, Tempe, Arizona 85281, USA

‡Corresponding author: jiefeng.sun@asu.edu

Abstract—Soft continuum robots can allow for biocompatible yet compliant motions, such as the ability of octopus arms to swim, crawl, and manipulate objects. However, current state-of-the-art continuum robots can only achieve real-time task-space control (i.e., tip control) but not whole-shape control, mainly due to the high computational cost from its infinite degrees of freedom. In this paper, we present a data-driven Koopman operator-based approach for the shape control of simulated multi-segment tendon-driven soft continuum robots with the Kirchhoff rod model. Using data collected from these simulated soft robots, we conduct a per-segment projection scheme on the state of the robots allowing for the identification of control-affine Koopman models that are an order of magnitude more accurate than without the projection scheme. Using these learned Koopman models, we use a linear model predictive control (MPC) to control the robots to a collection of target shapes of varying complexity. Our method realizes computationally efficient closed-loop control, and demonstrates the feasibility of real-time shape control for soft robots. We envision this work can pave the way for practical shape control of soft continuum robots.

I. INTRODUCTION

Soft continuum robotic arms, due to their continuous nature and compliant material constitution, are capable of producing biocompatible motions that enable non-destructive manipulation of delicate materials and safer interaction with humans than their rigid counterparts [17]. In particular, rigid robots are restricted by finite degrees of freedom and thus have limited applicability in applications that have diverse geometric constraints, such as in minimally invasive surgery [16], or when adapting to diverse environments [19]. Despite the geometrical advantages of soft robots, the efficient and robust control of the *shape* of soft robotic systems has been limited due to the difficulty in the high cost of dynamics prediction [7].

Physics-based models for soft robotic arms leverage nonlinear models that require high computational costs. Continuum mechanics models such as the Cosserat rod model [15, 25, 14] or the simpler Kirchhoff rod model [1] result in a system of partial differential equations (PDEs) that is computationally expensive to solve. Industrial finite element methods have also been employed for end-effector control [6], but the high spatial and temporal resolution needed to properly resolve

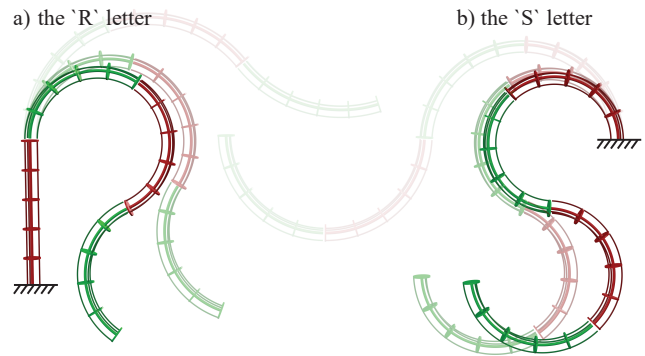


Fig. 1. A four-segment tendon-driven soft robot is controlled to move to the shapes of the letters “R” and “S”.

dynamics is often too computationally expensive for real-time control. Reduced order models are a popular alternative that greatly improves the computational speed of forward dynamics while preserving accuracy [9, 26]. However, they must rely on nonlinear control techniques that are slow to converge, especially for shape control where reference shapes must be high dimensional to sufficiently represent the desired geometries.

Data-driven models are a promising alternative to physics-based models that learn lightweight learnable operations to approximate the dynamics of a system, resulting in models that are more computationally efficient. Further, as the form of the model can be chosen by a user, they may, by construction, lend themselves to robust control algorithms. Deep neural networks have been shown to be an effective choice [23, 8, 28], although resulting controllers are significantly less interpretable than physics-based methods. Further, these heavyweight and nonlinear neural networks are often difficult to integrate into classical control frameworks for fast control and efficient optimization. In contrast, *Koopman operator*-based methods construct globally linear models of nonlinear systems, and thus can take advantage of linear control techniques [5, 12]. Recent research has demonstrated the growing success of Koopman-based methods in modeling and controlling soft robotic arms

[2, 3, 10, 20]. However, these works focus on control of the end effector, and as such, use low-dimensional state variables that are incapable of sufficiently representing the continuous shape of the robotic arm. Ref. [21] successfully leverages Koopman operators to control the shape of soft robotic arms, but makes the strong assumption that arbitrary forces can be applied at several points along the body of the robot.

In this paper, we leverage existing physics-based models to generate trajectory data for a collection of simulated soft robotic arms with realistic actuation forces. We then learn control affine Koopman operator-based models from the projected state variables of these collected trajectories, and then formulate an algorithm for controlling the shape of each soft robotic arm. For example, we can control a four segment robot to move to the shape of letters as in Fig. 1 (see supplementary video for more examples). The contributions of this work are as follows:

- 1) Development of a per-segment projection scheme for improved accuracy of Koopman models for soft robots.
- 2) Demonstrated shape control of tendon-driven soft robotic arms with between 1 and 5 independent segments.

The rest of the paper is organized as follows. In Sec. II, we provide relevant background information on Koopman operators and discrete Koopman operator identification. In Sec. III, we describe additional considerations made for the linear model predictive control (MPC) algorithm used in this work. In Sec. IV, we describe the simulated experimental setup, discuss the results of the control algorithm as applied to the simulated robots, and point out some limitations of the method. Lastly, in Sec. V, we provide some concluding remarks.

II. MATHEMATICAL FORMULATION

In this section, we provide a brief overview of applied Koopman operator theory and algorithms for data-driven identification of discrete-time Koopman operators.

A. Discrete-time Koopman Operators and Identification

Consider a dynamical system whose time evolution is described by

$$\dot{\mathbf{x}} = \mathbf{f}(\mathbf{x}, \mathbf{u}), \quad (1)$$

where $\mathbf{x} \in \mathbb{R}^n \equiv \mathcal{X}$ is the state of the system, $\dot{\mathbf{x}}$ denotes its time derivative, $\mathbf{u} \in \mathbb{R}^m \equiv \mathcal{U}$ are the control inputs of the system, and $\mathbf{f} : \mathcal{X} \times \mathcal{U} \rightarrow \mathcal{X}$ is a vector field describing the dynamics. In the case where the dynamics of \mathbf{x} is described by a system of PDEs, then \mathbf{f} can be considered an implicit function of the relevant derivatives of \mathbf{x} and \mathbf{u} . In discrete time, the system is propagated forward by the flow map $\mathbf{F}_t : \mathcal{X} \times \mathcal{U} \rightarrow \mathcal{X}$ defined by

$$\begin{aligned} \mathbf{x}(t_0 + t) &= \mathbf{F}_t(\mathbf{x}(t_0), \mathbf{u}(t_0)) \\ &= \mathbf{x}(t_0) + \int_{t_0}^{t_0+t} \mathbf{f}(\mathbf{x}(\tau), \mathbf{u}(\tau)) \, d\tau. \end{aligned} \quad (2)$$

When written using indices, the discrete time update can be written succinctly as

$$\mathbf{x}_{k+1} = \mathbf{F}_t(\mathbf{x}_k, \mathbf{u}_k). \quad (3)$$

The discrete-time Koopman operator \mathcal{K}_t is an infinite-dimensional linear operator that acts on functions $g : \mathcal{X} \times \mathcal{U} \rightarrow \mathbb{R}$ called *observables* which belong to some infinite-dimensional Hilbert space \mathcal{H} . In particular, the Koopman operator propagates state measurements forward in time using the forward flow map as

$$\mathcal{K}_t g = g \circ \mathbf{F}_t, \quad (4)$$

where \circ is the function composition operator. A common assumption to make Koopman operators amenable to linear control techniques is to assume that control inputs do not evolve forward over a single interval of time, i.e. $\dot{\mathbf{u}} = 0$ over (t_0, t_0+t) [3, 4]. In robotics, it is convenient to assume that the control inputs are not coupled with the robot dynamics, i.e. the time evolution of control inputs can be ignored or considered trivial. This is the case especially if they are fully specified by the user. By this assumption, we arrive at

$$\mathcal{K}_t g(\mathbf{x}_k, \mathbf{u}_k) = g(\mathbf{x}_{k+1}, \mathbf{u}_k). \quad (5)$$

Computing the full Koopman operator is infeasible as it is infinite dimensional. However, due to the fact that a Koopman-invariant subspace is spanned by a finite set of eigenfunctions of the Koopman operator, one can construct a globally linear representation of the nonlinear system using a finite set of functions [11]. To identify operators associated with these eigenfunctions, we first learn approximations of the Koopman operator on a finite set of basis functions. Consider a dataset $D = \{\mathbf{x}(t_i), \mathbf{x}(t_i + \Delta t), \mathbf{u}_i\}_{i=1}^N$ and a dictionary of scalar observables $\theta(\mathbf{x}, \mathbf{u}) : \mathcal{X} \times \mathcal{U} \rightarrow \mathbb{R}^M$. Dataset D yields three data matrices by stacking their respective column vectors, namely the state X , the next state X' after time shift Δt , and lastly the control input U . One can construct data matrices $\Theta(X, U)$ and $\Theta(X', U)$ where

$$\Theta(X, U) = \begin{bmatrix} \theta(\mathbf{x}(t_1), \mathbf{u}_1) & \dots & \theta(\mathbf{x}(t_N), \mathbf{u}_N) \\ \vdots & & \vdots \end{bmatrix}, \quad (6)$$

and $\Theta(X', U)$ is similarly defined, except applied to the state after time shift $\mathbf{x}(t_i + \Delta t)$. Then, a finite approximation of the discrete-time Koopman operator, denoted $K_{\Delta t}$, can be found by solving the related least squares problem

$$\begin{aligned} K_{\Delta t} &:= \underset{K_{\Delta t}^*}{\operatorname{argmin}} \|K_{\Delta t}^* \Theta(X, U) - \Theta(X', U)\|_2^2 \\ &\approx \Theta(X', U) \Theta^\dagger(X, U), \end{aligned} \quad (7)$$

where $(\cdot)^\dagger$ denotes the Moore-Penrose pseudoinverse. In this way, the left-eigenvectors of $K_{\Delta t}$ will be related to the finite set of eigenfunctions of the Koopman operator that span a Koopman-invariant subspace. This method is known as extended dynamic mode decomposition (EDMD) [27]. Eigenfunctions and eigenmodes can be directly extracted from

$K_{\Delta t}$ for more control over the model, but for simplicity, as done by [2, 3], we directly use $K_{\Delta t}$ to propagate the dictionary of functions θ forwards in time, as described by

$$\theta(\mathbf{x}_{k+1}, \mathbf{u}) \approx K_{\Delta t} \theta(\mathbf{x}_k, \mathbf{u}). \quad (8)$$

B. Practical Considerations

Computing the pseudoinverse in Eqn. (7) may be prone to overfitting, and is sensitive to outliers and noisy data during training [18]. To mitigate this issue, as suggested by Bruder et al. [2], we use the Least Absolute Shrinkage and Selection Operator (LASSO) [24]. This approach improves the sparsity of learned matrices by using an L^1 regularization, which is capable of driving terms to 0 and also tends to reduce the magnitude of eigenvalues, thereby improving the stability of the learned system. We modify Eqn. (7) as

$$K_{\Delta t} := \underset{K_{\Delta t}^*}{\operatorname{argmin}} \|K_{\Delta t}^* \Theta - \Theta'\|_2^2 + \alpha \|K_{\Delta t}^*\|_1, \quad (9)$$

where α is a hyperparameter that controls the magnitude of the regularization term, and we use the shorthand $\Theta \equiv \Theta(X, U)$ and $\Theta' \equiv \Theta(X', U)$.

III. CONTROL FORMULATION

Model predictive control (MPC) is a model-based controller design that features a finite time horizon, allowing the controller to anticipate future events. Importantly, for control affine systems, MPC yields a convex quadratic program which can be solved iteratively and with greater computational efficiency than their nonlinear counterpart [12]. To enable the use of this technique, we enforce our learned Koopman operator model to be control affine, namely by setting the dictionary of observables to be a concatenation of potentially nonlinear functions of \mathbf{x} with the identity function over \mathbf{u} . In particular, we let

$$\theta(\mathbf{x}, \mathbf{u}) = \begin{bmatrix} \theta_{\mathbf{x}}(\mathbf{x}) \\ \mathbf{u} \end{bmatrix}, \quad (10)$$

such that $\theta_{\mathbf{x}} : \mathbb{R}^n \rightarrow \mathbb{R}^{M-m}$ is some vector valued function of \mathbf{x} . Under the assumption that control inputs do not evolve forward in time, we may remove the last m rows of the learned operator corresponding to the time evolution of the control inputs, thus guaranteeing a control affine form of the learned Koopman operator, given by

$$\begin{aligned} \theta_{\mathbf{x}}(\mathbf{x}_{k+1}) &= [I_{M-m} \quad 0_{(M-m) \times m}] K_{\Delta t} \begin{bmatrix} \theta_{\mathbf{x}}(\mathbf{x}_k) \\ \mathbf{u}_k \end{bmatrix} \\ &= A \theta_{\mathbf{x}}(\mathbf{x}_k) + B \mathbf{u}_k, \end{aligned} \quad (11)$$

where $A \in \mathbb{R}^{(M-m) \times (M-m)}$, $B \in \mathbb{R}^{(M-m) \times m}$, and

$$K_{\Delta t} = \begin{bmatrix} A & B \\ 0_{m \times (M-m)} & I_m \end{bmatrix}. \quad (12)$$

Lastly, we define the MPC cost as the summation over a horizon of length H given by

$$\sum_{k=1}^H (C \mathbf{z}_{k+1} - \mathbf{r}_{k+1})^\top Q (C \mathbf{z}_{k+1} - \mathbf{r}_{k+1}) + \Delta \mathbf{u}_k^\top R \Delta \mathbf{u}_k. \quad (13)$$

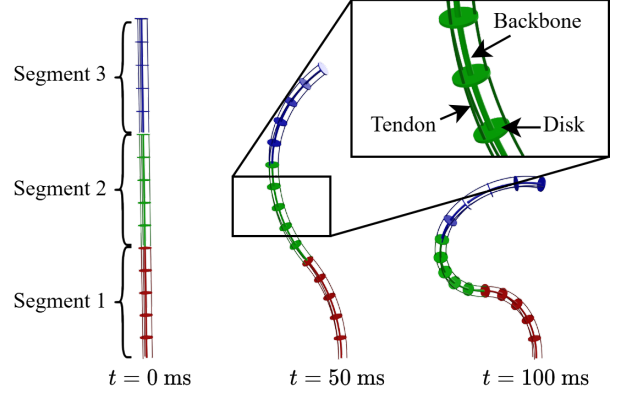


Fig. 2. Simulation setup of the 3-segment tendon-actuated robot

TABLE I
MATERIAL, GEOMETRICAL, AND SIMULATION PROPERTIES FOR EACH TENDON ROBOT CONFIGURATION

Parameter	Value
Length per segment (m)	1.0
Young's modulus (GPa)	200
Density (kg/m ³)	8000
Backbone radius (cm)	1.0
Number of tendons per segment	3
Tendon offset (cm)	4
Tendon angles (deg)	0, 120, 240
Spatial discretization per segment	100
Time step (s)	0.01

Here, $Q \in \mathbb{R}^{n \times n}$ and $R \in \mathbb{R}^{m \times m}$ are positive definite weight matrices chosen to penalize the different components of the state and control input vectors. Additionally, \mathbf{z}_k is the k th lifted state $\mathbf{z}_k = \theta_{\mathbf{x}}(\mathbf{x}_k)$, $\mathbf{r}_k \in \mathcal{X}$ is a reference shape, $\Delta \mathbf{u}_k = \mathbf{u}_{k+1} - \mathbf{u}_k$ is the change in control input, and C is a projection matrix such that $\mathbf{x}_k = C \mathbf{z}_k$. To guarantee that such C exists, we concatenate the state into the dictionary of functions by letting

$$C = [I_n \quad 0_{n \times (M-m-n)}], \quad \text{and} \quad \theta_{\mathbf{x}}(\mathbf{x}) = \begin{bmatrix} \mathbf{x} \\ \theta'_{\mathbf{x}}(\mathbf{x}) \end{bmatrix}, \quad (14)$$

for some vector valued function $\theta'_{\mathbf{x}} : \mathbb{R}^n \rightarrow \mathbb{R}^{M-m-n}$. To solve this quadratic program, we use the OSQP algorithm developed by Stellato et al. [22].

IV. NUMERICAL EXPERIMENTS

In this section, we conduct and analyze numerical experiments involving the shape control of a simulated tendon-driven soft robotic arm. In particular, we investigate the control of one, two, three, four, and five segment continuum arms, which have increasingly complex possible shapes.

A. Simulation Setup

Numerical simulations will be used to collect data for training the Koopman model and used as a testing environment for implementing the control. To simulate the soft arm, we separate it into its constituent parts, namely, the backbone, the tendons, and tendon routing disks as shown in Fig. 2.

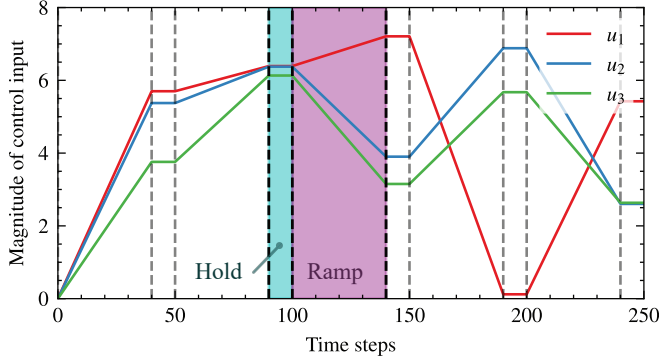


Fig. 3. Sample of ramp and hold timescales for control input sequences used when collecting trajectories for training Koopman operators

We model the backbone of the soft robot using the Kirchhoff rod model, subject to tendon forces described by Rucker and Webster III [15]. In particular, we use the implicit BDF- α method described by Till et al. [25] to solve for the continuum robot's dynamics. Under this discretization, the system of PDEs for the tendon actuated robot is

$$\begin{aligned}
 \mathbf{p}_t &= R\mathbf{q} \\
 R_t &= R\hat{\omega} \\
 \mathbf{v}_t &= \omega_s + \hat{\mathbf{v}}\omega \\
 \mathbf{q}_t &= \frac{1}{\rho A}R^T\mathbf{f} - \hat{\omega}\mathbf{q} \\
 \omega_t &= (\rho J)^{-1}(K_{bt}(\mathbf{v}_s - \mathbf{v}_s^*) + \hat{\mathbf{v}}K_{bt}(\mathbf{v} - \mathbf{v}^*) \\
 &\quad + R^T\mathbf{l} - \hat{\omega}\rho J\omega)
 \end{aligned} \tag{15}$$

where \mathbf{p} is the position of the backbone with respect to arclength s , R is the orientation along the backbone, \mathbf{v} is the angular strain, \mathbf{q} is the linear velocity, and ω is the angular velocity. The subscripts $(\cdot)_s$ and $(\cdot)_t$ denote partial derivatives with respect to arclength s and time t . The superscript $(\cdot)^*$ denotes the variables value in the reference configuration. The operator $\hat{\cdot}$ denotes the mapping from \mathbb{R}^3 to $\mathfrak{se}(3)$. Further, we let ρ denote the density of the backbone material, A denote the area of its cross section, J be the matrix of second area moments of the cross section, K_{bt} be the stiffness matrix for bending and torsion, and $\mathbf{f}, \mathbf{l} \in \mathbb{R}^3$ be the external forces and moments due to external loads and tendon actuation forces. For more details on the BDF- α method, the evaluation of tendon forces, and all relevant boundary conditions, we refer the reader to Till et al. [25]. The solutions to Eqn. (15) are used as the ground truth in the control experiments, and are collected for use as trajectories when learning Koopman operators.

As shown in Fig. 2, the reference shape of the backbone is assumed to be straight and cylindrical, and all tendons are routed parallel to the backbone. Each segment has their own set of tendons which only apply forces along the length of that segment. All other relevant material, geometrical, and simulation properties are summarized in Table I.

B. Data Collection

For each robot, 480 trajectories including 120,000 snapshots $(\mathbf{x}(t), \mathbf{x}(t + \Delta t), \mathbf{u}(t))$ are collected. To collect the data, we

first initialize the robot to its steady state in absence of control inputs. In particular, we let the control input \mathbf{u} be a vector of the forces applied to each tendon, and initially set $\mathbf{u}(0) = 0$. Then, we randomly sample 5 unique control inputs from \mathbb{R}^M by sampling each component from a uniform distribution $\mathcal{U}(0, 8)$ in Newtons, where $\mathcal{U}(a, b)$ denotes a uniform distribution between minimum value a and maximum value b . We denote these 5 control inputs as \mathbf{u}_i for $i \in \{1, \dots, 5\}$. Then, as a function of the simulation clock time t , we allow control inputs to linearly interpolate or ramp between each consecutive \mathbf{u}_i for time t_r before holding them fixed at \mathbf{u}_i for time t_h . Specifically, we define, for $t \in [0, 5(t_r + t_h)]$,

$$\mathbf{u}(t) = \begin{cases} \mathbf{u}_i(1 - \theta) + \mathbf{u}_{i+1}\theta & t - t_0 < t_r \\ \mathbf{u}_{i+1} & t_r \leq t - t_0 < t_h \end{cases}, \tag{16}$$

where $\tau_0 = 0$, and we define $i = \lfloor t/(t_r + t_h) \rfloor$, $t_0 = (t_r + t_h)i$, and $t_1 = (t_r + t_h)(i + 1)$. The interpolation parameter θ is defined as

$$\theta = \frac{t - t_0}{t_1 - t_0}. \tag{17}$$

In particular, we define $\Delta t = 0.01s$, $t_r = 40\Delta t$ and $t_h = 10\Delta t$. After ramping to and holding at each of the 5 randomly selected control inputs, we then terminate the simulation, and run another. A sample of the control inputs used in one of the 480 trajectories used for the one segment robot is shown in Fig. 3. Snapshots are generated by subsampling from these simulations, where \mathbf{x} is computed as described in the following Sec. IV-C.

C. Koopman Identification and Per-segment Projection

The Koopman operators used are learned using the data-driven identification method described in Sec. II-A. In line with the control affine assumption given by Eqn. (10), we choose $\theta_{\mathbf{x}}(\mathbf{x})$ to be an impure function yielding two time-delayed coordinates of \mathbf{x} , such that

$$\theta_{\mathbf{x}}(\mathbf{x}_k) = \begin{bmatrix} \mathbf{x}_k \\ \mathbf{x}_{k-1} \\ \mathbf{x}_{k-2} \end{bmatrix}. \tag{18}$$

We define the control input vector $\mathbf{u} \in \mathbb{R}^m$ as the tension applied to each tendon, where m is the total number of tendons. The ordering of these control inputs is arbitrary, however, for consistency, they are ordered first by increasing segment index, and then by increasing angle 0° , 120° , and 240° . As a control input to the Koopman operator, one might also choose $\Delta\mathbf{u}_k = \mathbf{u}_k - \mathbf{u}_{k-1}$ over \mathbf{u}_k due to the fact that it is zero centered.

A natural choice of state variable $\mathbf{x} \in \mathbb{R}^n$ is a concatenation of several positions \mathbf{p} along the backbone such that $n = 3\bar{p}$, where \bar{p} is the number of points subsampled from the backbone. This allows for trivial comparison with a reference shape, as long as the curve is also defined by positions in space. Additionally, position tends to be easier to observe in practice (i.e. with motion capture cameras), and omitting the orientation R and other state variables enables smaller dimensionality of the learned operators.

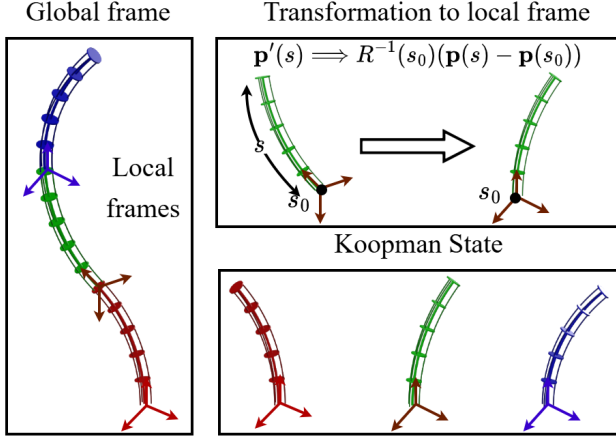


Fig. 4. Projection of each segment in the three segment robot onto their local coordinate frame

However, naively choosing this set of state variables leads to large model errors due to the control affine assumption. Indeed, small changes in the control input for segments closer to the fixed end of the robotic arm leads to highly nonlinear dynamics at the distal end. Instead, as each segment has their own independent set of tendons, one can project each segment into its local coordinate frame, and use the resulting coordinates to learn the corresponding Koopman operator. This procedure guarantees that the effect of tendon forces applied to a segment closer to the fixed end is minimal on a segment near the distal end, promoting sparsity of the control input Koopman matrix. In particular, we assign to each position along the arclength s of the backbone,

$$\mathbf{p}'(s) \implies R^{-1}(s_0)(\mathbf{p}(s) - \mathbf{p}(s_0)), \quad (19)$$

where $\mathbf{p}'(s)$ is the transformed position coordinate, and s_0 is the position along the arclength of the backbone where the segment originates. This procedure is summarized by Fig. 4. To further reduce dimensionality, 10 position vectors are taken uniformly from each segment instead of using the full discretization used in the simulations.

In Fig. 5, we compare the mean squared unprojected shape error of each choice of Koopman model as a function of the prediction horizon. The error is computed over 200 trajectories with 200 time steps, each collected separately from the training of the Koopman operator. We find that using $\Delta \mathbf{u}$ with the aforementioned projection scheme leads to models with the highest accuracy. For consistency, the full state of the non-projected models are reconstructed from the Koopman state by including orientations $R(s_0)$ for each segment and inverting the procedure described by Eqn. (19). Error is then computed at each discretized point s_i along the backbone using the mean squared shape error (MSE) given by

$$\text{MSE} = \frac{1}{n} \sum_{i=1}^n \|\mathbf{p}(s_i) - \mathbf{p}_{\text{ref}}(s_i)\|_2^2, \quad (20)$$

where $\mathbf{p}(s)$ denotes the position of the simulated backbone

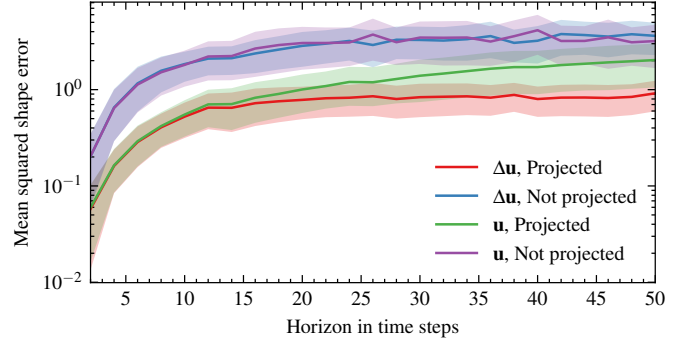


Fig. 5. Mean and 1 standard deviation range of the mean squared shape error of Koopman models as a function of the length of horizon. Models are trained in the case of a three segment robot. $\Delta \mathbf{u}$ or \mathbf{u} refers to using the respective value as the control input in the Koopman operator. Projected or not projected refers to using or not using the projection scheme described by Eqn. (19)

as a function of arclength, and $\mathbf{p}_{\text{ref}}(s)$ is the position of the reference shape as a function of arclength. In all figures the MSE will be plotted on a semilog plot.

D. Results

In our numerical experiments, we provide a static reference shape and observe the resulting dynamical trajectories the soft robot takes to obtain the correct result. To generate these reference shapes, we solve the corresponding static equilibrium equations derived from Eqn. (15) for some fixed and randomly selected value of \mathbf{u} . For each method, we observe and compare the time to convergence and the quality of the trajectory in the neighborhood of the reference shape.

Fig. 6 showcases several snapshots of the backbone and the loss curve for three example trajectories from the 3, 4, and 5 segment robots. In each case, the final shape of the robot is qualitatively and quantitatively very close to the reference shape, demonstrating the efficacy of the developed method. The shaded pink regions highlight the 2nd half of the simulation, which showcases the different types of observed convergence behavior. In Fig. 6.g, a jump in the error is observed at around 150 time steps, corresponding to large dynamical errors in the Koopman model. In several cases, such as in Fig. 6.a, b, c, and i, the Koopman model error causes a spike in the shape error between 60 and 70 time steps. In Fig. 6.e we see this spike occurs in the 2nd half of the simulation after the robot appears to have initially converged. Despite these model errors affecting the stability, the final shape error is consistently improved by over 2 orders of magnitude.

For each robot and for each of three tested controllers, 200 simulations of 200 time steps each are conducted and the shape error of each controller is computed. First, we test the controller with a model that does not use the projection scheme. Then, we test two controllers using the projection scheme that use two different choices for the gain matrix Q . As shown in Fig. 7, the control algorithm with the projection method is able to consistently improve the shape error between the robot and a reference shape by several orders of magnitude

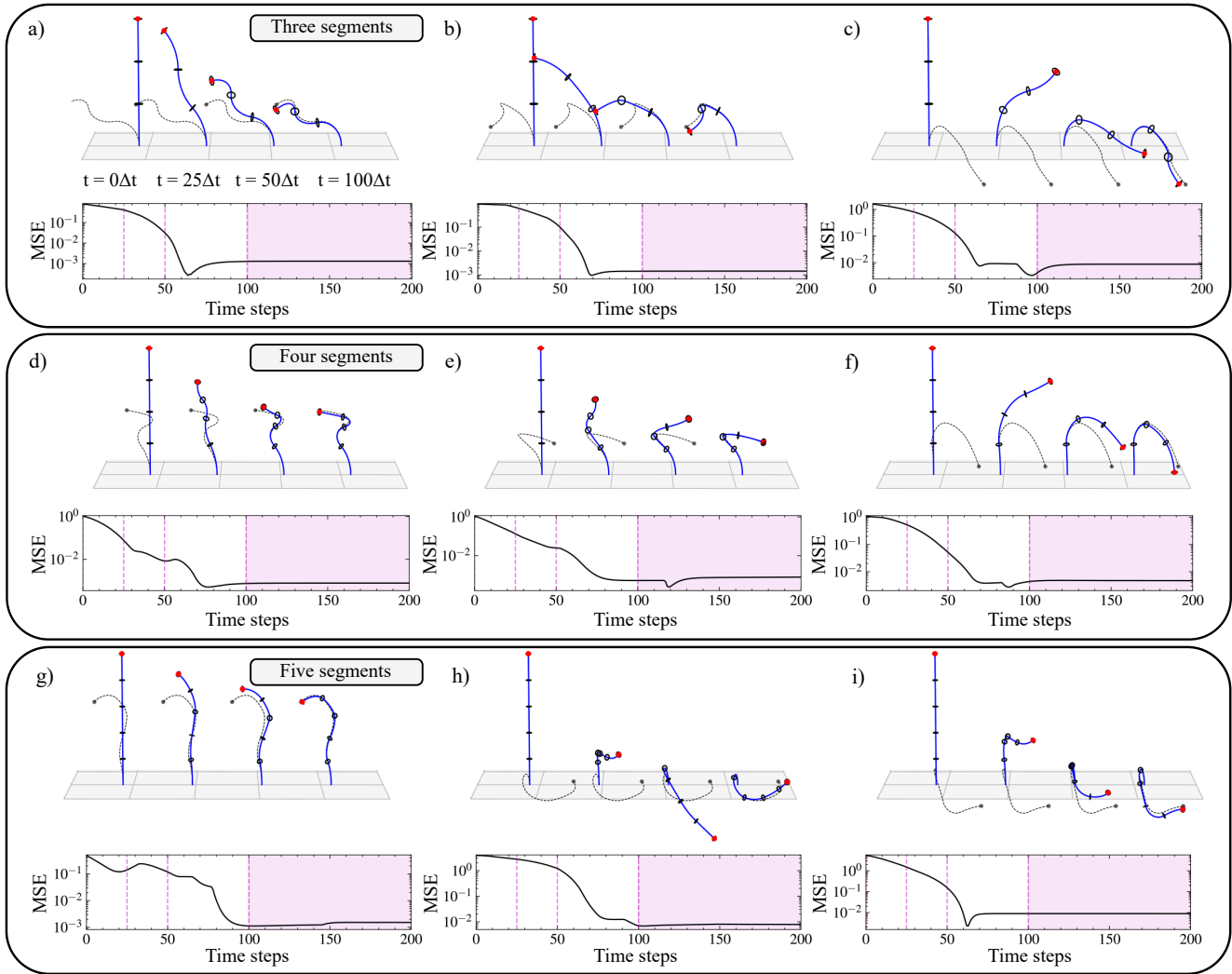


Fig. 6. Sample trajectories of the 3 (a-c), 4 (d-f), and 5 (g-i) segment robots shown in blue for three different reference shapes shown as dashed black lines (see supplementary video). Plotted below is the mean squared shape error as a function of the number of time steps. Dashed pink lines denote where the trajectory snapshots are taken. The highlighted pink regions denote the 2nd half of the simulation, where most trajectories have already converged.

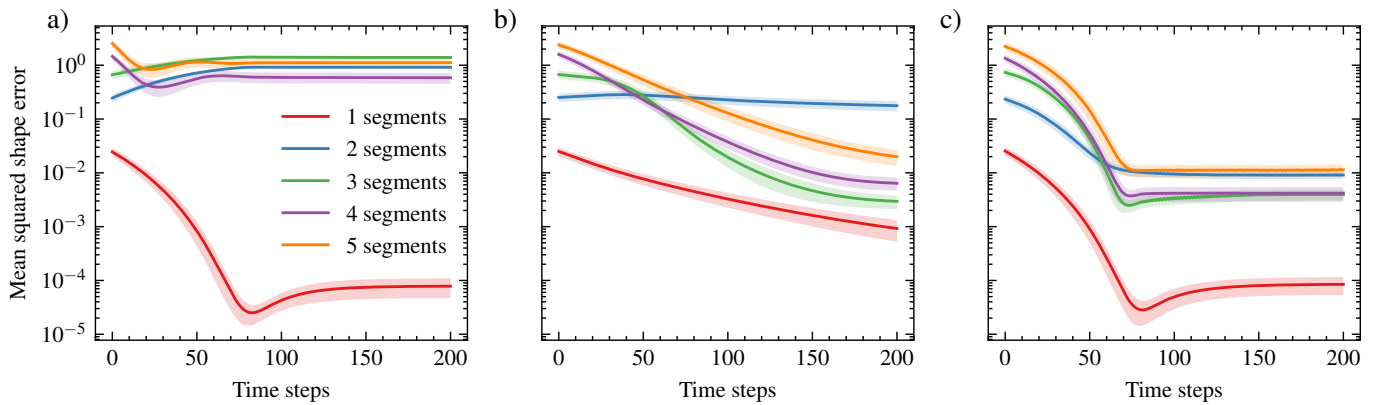


Fig. 7. Mean and 0.25 standard deviation range of the mean squared shape error for different methods. a) is the shape error using a weighted Q matrix described by Eqn. (21) without using the projection scheme. b) uses Q proportional to the identity matrix with the projection scheme, while c) uses a weighted Q matrix described by Eqn. (21) with the projection scheme. Quarter standard deviations are chosen to ensure nonnegativity on the semi-log plot.

over a period two seconds in real time. When the projection method is not used, the shape error of the multiple segment robots is not able to improve as seen in Fig. 7.a. Further, when using the projection method, the convergence behavior is heavily dependent on the choice of gain matrix Q . Fig. 7.b and Fig. 7.c showcase two principled choices of Q , where Q is a rescaled identity matrix $Q = 20I$ and where Q is a weighted diagonal matrix respectively. The weighted Q matrix features larger terms for segments closer to the fixed end, and smaller terms for segments near the distal end, given by

$$Q = 20(\text{diag} \circ \text{vec}) \left(\begin{pmatrix} \bar{p} & \bar{p} - 1 & & 1 \\ \bar{p} & \bar{p} - 1 & \dots & 1 \\ \bar{p} & \bar{p} - 1 & & 1 \end{pmatrix} \right). \quad (21)$$

Here, diag denotes the diagonalization operation, vec denotes the vectorization operation. This second choice of Q , although promoting faster convergence, demonstrates the steady state model error inherent to Koopman models of this type, described more clearly in Sec. IV-E.

E. Limitations

Identified Koopman operator models, especially in low data limits, tend to yield spurious eigenvalues [13], and as a consequence, tend to have instability issues when used naively. In particular, due to model inaccuracies, the steady states of the data-driven model for a fixed control input may be prohibitively inaccurate in comparison to the true steady states of the system [10]. In general, the learned Koopman models, for a fixed control input, are generally unable to converge to the correct steady state, even in trivial cases. For example, in the case where the robot starts in its initial configuration, and no work is done by the control inputs, a significant amount of deviation is observed from the initial configuration, as shown in Fig. 8. This effect is reflected by nearly any configuration in the dynamical manifold. As a consequence of these model errors, the MPC controller is unable to maintain the lowest obtainable error as shown in Fig. 7, which has a large dip in the shape error between 50 and 100 time steps. Principled ways to address this steady state error have begun to appear in literature, such as the work done by Haggerty et al. [10], which uses a specially designed static Koopman operator as a pre-gain term for optimal control. Taking advantage of such techniques will likely have a strong impact towards addressing this issue.

V. CONCLUSION

In this paper, we have employed a data-driven method to control the shape of tendon-driven continuum soft robots using control affine Koopman models and linear MPC. We show that this method is able to successfully control multi-segment tendon-actuated soft robotic arms by using a per-segment projection, robustly handling the highly nonlinear dynamics that arise from the system.

While these results are promising, they hint at many areas which may require further work. Principled choices of dictionary functions remain an open problem that varies from system

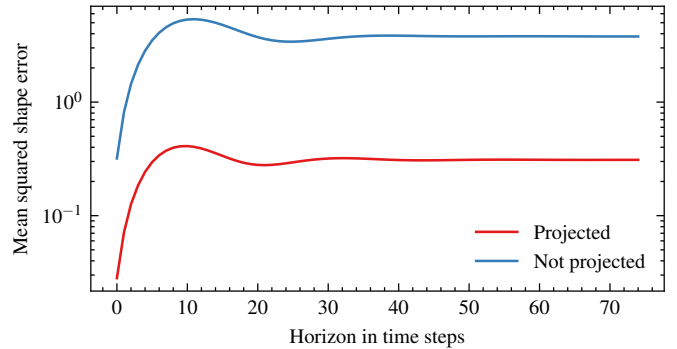


Fig. 8. Norm of the steady state error for the Koopman model of the three segment robot when control inputs are fixed at 0 as a function of the number of time steps.

to system. Further, the large steady-state error of the Koopman model and high data requirements of Koopman models are problems that may limit the practical application of this class of methods to physical prototypes. As such, in future work, we would like to experimentally validate this approach on physical prototypes, using models learned from characterized and simulated data as in this work, as well as models learned from observed trajectories of the physical prototype itself.

REFERENCES

- [1] Jiali Bao, Weihang Chen, and Jing Xu. Kinematics Modeling of a Twisted and Coiled Polymer-Based Elastomer Soft Robot. *IEEE Access*, 7:136792–136800, 2019. ISSN 2169-3536. doi: 10.1109/ACCESS.2019.2942486. Conference Name: IEEE Access.
- [2] Daniel Bruder, Brent Gillespie, C. David Remy, and Ram Vasudevan. Modeling and Control of Soft Robots Using the Koopman Operator and Model Predictive Control. *Robotics: Science and Systems XV*, June 2019. doi: 10.15607/RSS.2019.XV.060. Conference Name: Robotics: Science and Systems 2019 ISBN: 9780992374754 Publisher: Robotics: Science and Systems Foundation.
- [3] Daniel Bruder, Xun Fu, R. Brent Gillespie, C. David Remy, and Ram Vasudevan. Data-Driven Control of Soft Robots Using Koopman Operator Theory. *IEEE Transactions on Robotics*, 37(3):948–961, June 2021. ISSN 1941-0468. doi: 10.1109/TRO.2020.3038693. Conference Name: IEEE Transactions on Robotics.
- [4] Daniel Bruder, Xun Fu, R. Brent Gillespie, C. David Remy, and Ram Vasudevan. Koopman-Based Control of a Soft Continuum Manipulator Under Variable Loading Conditions. *IEEE Robotics and Automation Letters*, 6(4):6852–6859, October 2021. ISSN 2377-3766. doi: 10.1109/LRA.2021.3095268. Conference Name: IEEE Robotics and Automation Letters.
- [5] Daniel Bruder, Xun Fu, and Ram Vasudevan. Advantages of Bilinear Koopman Realizations for the Modeling and Control of Systems With Unknown Dynamics. *IEEE Robotics and Automation Letters*, 6(3):4369–4376, July 2021. ISSN 2377-3766, 2377-3774. doi: 10.1109/LRA.2021.3068117.

- [6] Christian Duriez. Control of elastic soft robots based on real-time finite element method. In *2013 IEEE International Conference on Robotics and Automation*, pages 3982–3987, May 2013. doi: 10.1109/ICRA.2013.6631138. ISSN: 1050-4729.
- [7] Thomas George Thuruthel, Yasmin Ansari, Egidio Falotico, and Cecilia Laschi. Control Strategies for Soft Robotic Manipulators: A Survey. *Soft Robotics*, 5(2):149–163, January 2018. ISSN 2169-5172. doi: 10.1089/soro.2017.0007. Publisher: Mary Ann Liebert, Inc., publishers.
- [8] Morgan T. Gillespie, Charles M. Best, Eric C. Townsend, David Wingate, and Marc D. Killpack. Learning nonlinear dynamic models of soft robots for model predictive control with neural networks. In *2018 IEEE International Conference on Soft Robotics (RoboSoft)*, pages 39–45, April 2018. doi: 10.1109/ROBOSOFT.2018.8404894.
- [9] Olivier Goury and Christian Duriez. Fast, Generic, and Reliable Control and Simulation of Soft Robots Using Model Order Reduction. *Trans. Rob.*, 34(6):1565–1576, December 2018. ISSN 1552-3098. doi: 10.1109/TRO.2018.2861900.
- [10] David A. Haggerty, Michael J. Banks, Ervin Kamenar, Alan B. Cao, Patrick C. Curtis, Igor Mezić, and Elliot W. Hawkes. Control of soft robots with inertial dynamics. *Science Robotics*, 8(81):eadd6864, August 2023. doi: 10.1126/scirobotics.add6864. Publisher: American Association for the Advancement of Science.
- [11] Eurika Kaiser, J Nathan Kutz, and Steven L Brunton. Data-driven discovery of Koopman eigenfunctions for control. *Machine Learning: Science and Technology*, 2(3):035023, September 2021. ISSN 2632-2153. doi: 10.1088/2632-2153/abf0f5.
- [12] Milan Korda and Igor Mezić. Linear predictors for nonlinear dynamical systems: Koopman operator meets model predictive control. *Automatica*, 93:149–160, July 2018. ISSN 0005-1098. doi: 10.1016/j.automatica.2018.03.046.
- [13] Joshua L. Proctor, Steven L. Brunton, and J. Nathan Kutz. Generalizing Koopman Theory to Allow for Inputs and Control. *SIAM Journal on Applied Dynamical Systems*, 17(1):909–930, January 2018. doi: 10.1137/16M1062296. Publisher: Society for Industrial and Applied Mathematics.
- [14] Federico Renda, Michele Giorelli, Marcello Calisti, Matteo Cianchetti, and Cecilia Laschi. Dynamic Model of a Multibending Soft Robot Arm Driven by Cables. *IEEE Transactions on Robotics*, 30(5):1109–1122, October 2014. ISSN 1941-0468. doi: 10.1109/TRO.2014.2325992. Conference Name: IEEE Transactions on Robotics.
- [15] D. Caleb Rucker and Robert J. Webster III. Statics and Dynamics of Continuum Robots With General Tendon Routing and External Loading. *IEEE Transactions on Robotics*, 27(6):1033–1044, December 2011. ISSN 1941-0468. doi: 10.1109/TRO.2011.2160469. Conference Name: IEEE Transactions on Robotics.
- [16] Mark Runciman, Ara Darzi, and George P. Mylonas. Soft Robotics in Minimally Invasive Surgery. *Soft Robotics*, 6(4):423–443, March 2019. ISSN 2169-5172. doi: 10.1089/soro.2018.0136. Publisher: Mary Ann Liebert, Inc., publishers.
- [17] Daniela Rus and Michael T. Tolley. Design, fabrication and control of soft robots. *Nature*, 521(7553):467–475, May 2015. ISSN 1476-4687. doi: 10.1038/nature14543. Publisher: Nature Publishing Group.
- [18] Allan Seheult, P. Green, Peter Rousseeuw, and Annick Leroy. Robust Regression and Outlier Detection. *Journal of the Royal Statistical Society. Series A (Statistics in Society)*, 152:133, January 1989. doi: 10.2307/2982847.
- [19] Dylan S. Shah, Joshua P. Powers, Liana G. Tilton, Sam Kriegman, Josh Bongard, and Rebecca Kramer-Bottiglio. A soft robot that adapts to environments through shape change. *Nature Machine Intelligence*, 3(1):51–59, January 2021. ISSN 2522-5839. doi: 10.1038/s42256-020-00263-1. Publisher: Nature Publishing Group.
- [20] Lu Shi, Zhichao Liu, and Konstantinos Karydis. Koopman Operators for Modeling and Control of Soft Robotics. *Current Robotics Reports*, 4(2):23–31, June 2023. ISSN 2662-4087. doi: 10.1007/s43154-023-00099-8.
- [21] Ajai Singh, Jiefeng Sun, and Jianguo Zhao. Controlling the Shape of Soft Robots Using the Koopman Operator. In *2023 American Control Conference (ACC)*, pages 153–158, May 2023. doi: 10.23919/ACC55779.2023.10156145. ISSN: 2378-5861.
- [22] Bartolomeo Stellato, Goran Banjac, Paul Goulart, Alberto Bemporad, and Stephen Boyd. OSQP: an operator splitting solver for quadratic programs. *Mathematical Programming Computation*, 12(4):637–672, December 2020. ISSN 1867-2957. doi: 10.1007/s12532-020-00179-2.
- [23] Thomas George Thuruthel, Egidio Falotico, Federico Renda, and Cecilia Laschi. Model-Based Reinforcement Learning for Closed-Loop Dynamic Control of Soft Robotic Manipulators. *IEEE Transactions on Robotics*, 35(1):124–134, February 2019. ISSN 1941-0468. doi: 10.1109/TRO.2018.2878318. Conference Name: IEEE Transactions on Robotics.
- [24] Robert Tibshirani. Regression Shrinkage and Selection via the Lasso. *Journal of the Royal Statistical Society. Series B (Methodological)*, 58(1):267–288, 1996. ISSN 0035-9246. Publisher: [Royal Statistical Society, Oxford University Press].
- [25] John Till, Vincent Aloï, and Caleb Rucker. Real-time dynamics of soft and continuum robots based on Cosserat rod models. *The International Journal of Robotics Research*, 38(6):723–746, May 2019. ISSN 0278-3649. doi: 10.1177/0278364919842269. Publisher: SAGE Publications Ltd STM.
- [26] Sander Tonkens, Joseph Lorenzetti, and Marco Pavone.

Soft Robot Optimal Control Via Reduced Order Finite Element Models. *2021 IEEE International Conference on Robotics and Automation (ICRA)*, pages 12010–12016, May 2021. doi: 10.1109/ICRA48506.2021.9560999. Conference Name: 2021 IEEE International Conference on Robotics and Automation (ICRA) ISBN: 9781728190778 Place: Xi'an, China Publisher: IEEE.

- [27] Matthew O. Williams, Ioannis G. Kevrekidis, and Clarence W. Rowley. A Data-Driven Approximation of the Koopman Operator: Extending Dynamic Mode Decomposition. *Journal of Nonlinear Science*, 25(6): 1307–1346, December 2015. ISSN 1432-1467. doi: 10.1007/s00332-015-9258-5.
- [28] Gang Zheng, Yuan Zhou, and Mingda Ju. Robust control of a silicone soft robot using neural networks. *ISA Transactions*, 100:38–45, May 2020. ISSN 0019-0578. doi: 10.1016/j.isatra.2019.12.004.